2011 American Control Conference
on O'Farrell Street, San Francisco, CA, USA
June 29 - July 01, 2011

Control-Oriented Modeling of Diesel Engine Gas Exchange

Lyle Kocher, Ed Koeberlein, Karla Stricker, D. G. Van Alstine, Brandon Biller, and Gregory M. Shaver

Abstract— **Modeling and control of the gas exchange process in modern diesel engines is critical for the promotion and control of advanced combustion strategies. However, most modeling efforts to date use complex stand-alone simulation packages that are not easily integrated into, or amenable for the synthesis of, engine control systems. Simpler control-oriented models have been developed, however in many cases they do not directly capture the complete dynamic interaction of air handling system components and flows in multi-cylinder diesel engines with variable geometry turbocharging and high pressure exhaust gas recirculation. This paper describes a simple, low order model of the air handling system for a multi-cylinder turbocharged diesel engine with cooled exhaust recirculation, validated against engine test data.**

I. INTRODUCTION

Current and future emissions regulations and demand for improved fuel economy have necessitated the development of more complex engine systems and control strategies, as well as novel combustion techniques aimed at reducing emissions while maintaining efficiency [1], [2], [3], [4]. The development and use of these advanced combustion techniques require increasingly accurate and robust control of the gas exchange process [5], [6], [7]. Cost and time intensive engine testing has generally been a large part of engine control optimization, motivating the need for analysis-led design and a more complete understanding of the gas exchange process and dynamics of the air handling system [8], [9].

While physics-based engine simulation models have been used extensively for years for design and performance prediction, a relatively small number are amenable to control design and have been developed to the extent of completely characterizing air handling systems for diesel engine control [10]. Much of the prior modeling efforts, while accurately describing the dynamic interaction of engine components, make use of detailed engine models via simulation packages such as GT-Power [11], [12], [13], [14], [15]. These models, while accurate in their predictive capabilities, are generally more complex than is feasible for control design. Control-oriented models have also been developed [16], [17], [18], [19], [20].

The aim of this work is the development of a control-amenable engine model that can be used for real-time control systems and that captures the behavior of the engine across its entire operating space. A complete characterization of the air handling system of a modern diesel engine with cooled exhaust gas recirculation (EGR), a variable geometry turbocharger (VGT) and charge air cooler (CAC) is presented, along with experimental validation of the model during both steady state and transient operation.

II. EXPERIMENTAL SETUP

The air handling system model developed here is validated against engine data from a Cummins diesel engine outfitted with a variable valve actuation (VVA) system. The engine used is a direct-injection in-line 6-cylinder Cummins ISB with a displacement of 6.7 liters, 350 horsepower, and a geometric compression ratio of 17.3:1. The engine's air-handling system consists of a VGT and EGR valve. Flow into and out of the cylinder is regulated with a pair of exhaust valves and a pair of intake valves per cylinder. The exhaust valves are driven by the camshaft; however, the intake valves are driven by the electro-hydraulic VVA system matching the standard camshaft intake valve profile. Boosted fresh air from the turbocharger is cooled with a charge air cooler. The fuel system consists of a Bosch common rail fuel injection system with multi-pulse injection capabilities.

Engine data used for model validation was acquired using a dSPACE system. The dSPACE system collects available data from the electronic control module (ECM), such as fueling commands, as well as from additional temperature, pressure, emissions, and flow measurements instrumented on the engine test bed. Cummins proprietary software is utilized to access and control the ECM and command the positions of the EGR valve and the VGT nozzle. Emissions gas analzyers are used to measure the composition of the exhaust gases as well as the concentration of CO_2 in the intake manifold. EGR fraction is calculated using the CO_2 measurements of the intake and exhaust streams. Cambustion NDIR Fast CO_2 Analyzers were utilized during transient tests for their fast response times of 8 ms. With the short response time, the analyzers are fast enough to capture the transient responses used for simulation validation. Steady state CO_2 data was collected using a California Analytical Instruments NDIR gas analyzer.

III. CONTROL ORIENTED MODEL

This section outlines a physically motivated reduced order model of the air handling system of a diesel engine to ultimately be used for control design. The model consists of 7 states: temperature and pressure of the intake manifold and exhaust manifold, pressure of EGR cooler and CAC, as well as the turbocharger shaft speed. The states are shown visually in Figure 1. Using the ideal gas law, the mass of each manifold is a function of the other manifold states and volume.

A. Intake and Exhaust Manifold Models

The intake and exhaust manifolds are both modeled with the commonly used manifold filling dynamics approach [1],

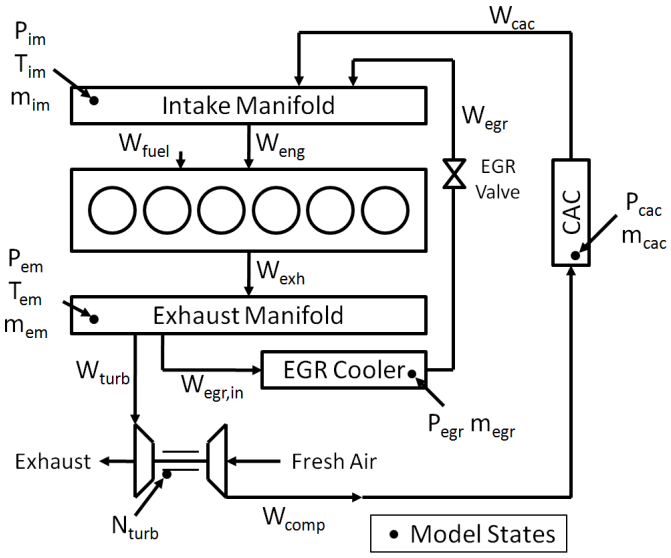

Fig. 1. Schematic of a modern diesel engine denoting model states and flow variables.

[17], [21]. The intake manifold is considered to be the volume between the CAC outlet and the piston-cylinder volume. All thermodynamic states are assumed to be constant throughout the volume. The governing equations for the intake manifold are:

$$\frac{dP_{im}}{dt} = \frac{\gamma_{im} R_{im}}{V_{im}} (W_{egr} T_{egr} + W_{cac} T_{cac} - W_{eng} T_{im}) \tag{1}$$

$$\begin{aligned} \frac{dT_{im}}{dt} &= \frac{T_{im} R_{im}}{P_{im} V_{im} c_{v,amb}} [W_{egr} T_{egr} c_{p,exh} \\ &+ W_{cac} T_{cac} c_{p,amb} - W_{eng} T_{im} c_{p,amb} \\ &- (W_{egr} + W_{cac} - W_{eng}) T_{im} c_{v,amb}] \end{aligned} \tag{2}$$

where T, P, and V denote temperature, pressure, and volume respectively at the subscripted state location. System flows are represented by W. Subscripts im, egr, and cac refer to the properties of the model relating to the intake manifold, EGR cooler, and the CAC, respectively. All system flows and states are shown in Figure 1. The specific heats $c_{p,amb}$ and $c_{p,exh}$ are the specific heats at constant pressure for ambient air and exhaust gas, respectively, and $c_{v,amb}$ is the specific heat at constant volume for ambient air. γ_{im} is the ratio of the specific heats for the conditions found in the intake manifold.

Flow from the intake manifold into the cylinders, W_{eng}, is modeled using the speed-density equation [22],

$$W_{eng} = \frac{1}{2} \rho_{im} \eta_v V_d N \tag{3}$$

where ρ_{im} is the density of air in the intake manifold, η_v is the volumetric efficiency, V_d is the displacement volume, and N is the engine speed.

The volumetric efficiency is computed using an experimentally derived model in which $\eta_v = \eta_v(P_{im}, T_{im}, P_{em})$, where P_{em} is the exhaust manifold pressure.

The exhaust manifold is defined as the lumped volume between the piston cylinder volume, the EGR cooler, and the turbocharger inlet. The modeling of the exhaust manifold is similar to that of the intake manifold:

$$\frac{dP_{em}}{dt} = \frac{\gamma_{exh} R_{exh}}{V_{em}} ((W_{eng} + W_{fuel}) T_{exh} - W_{egr,in} T_{em} - W_{turb} T_{em}) \tag{4}$$

$$\begin{aligned} \frac{dT_{em}}{dt} &= \frac{T_{em} R_{em}}{P_{em} V_{em} c_{v,exh}} [(W_{eng} + W_{fuel}) T_{exh} c_{p,exh} \\ &- W_{egr} T_{em} c_{p,exh} - W_{turb} T_{em} c_{p,exh} \\ &- (W_{eng} + W_{fuel} - W_{egr,in} - W_{turb}) T_{em} c_{v,exh}] \end{aligned} \tag{5}$$

where R_{em} is the gas constant for the composition in the exhaust manifold and T_{exh} is the temperature of the gas flowing out from the cylinder. Similar to the volumetric efficiency model, T_{exh} is calculated from an experimentally derived model where $T_{exh} = T_{exh}(AFR)$ where AFR is the air-to-fuel ratio.

B. EGR Valve

EGR flow is modeled as a function of the upstream and downstream pressure of the EGR valve using the standard orifice flow equation [17]:

$$W_k = \begin{cases} CA_{eff} \frac{p_i}{\sqrt{RT_i}} \Psi\left(\frac{p_j}{p_i}\right) & \text{if } p_j < p_i \\ 0 & \text{if } p_1 = p_2 \\ CA_{eff} \frac{p_j}{\sqrt{RT_j}} \Psi\left(\frac{p_i}{p_j}\right) & \text{if } p_j > p_i \end{cases} \tag{6}$$

Here, k can be replaced with egr to describe EGR flow, and subscripted indices i and j correspond to the upstream flow conditions and downstream flow conditions, respectively. In this case, upstream conditions are taken to be that of the EGR cooler exit while downstream conditions are that of the intake manifold. C is the discharge coefficient associated with the valve opening and A_{eff} is the effective flow area, which is a function of the EGR valve position. The pressure ratio correction factor, Ψ, is given by

$$\Psi\left(\frac{p_i}{p_j}\right) = \begin{cases} \sqrt{\gamma} \left(\frac{2}{\gamma+1}\right)^{((\gamma+1)/2(\gamma-1))} \\ \text{if } \frac{p_i}{p_j} \le \left(\frac{2}{\gamma+1}\right)^{\gamma/(\gamma-1)} \\ \sqrt{\frac{2\gamma}{\gamma-1} \left(\left(\frac{p_i}{p_j}\right)^{2/\gamma} - \left(\frac{p_i}{p_j}\right)^{(\gamma+1)/\gamma} \right)} \\ \text{if } \frac{p_i}{p_j} > \left(\frac{2}{\gamma+1}\right)^{\gamma/(\gamma-1)} \end{cases} \tag{7}$$

where γ corresponds to the ratio of specific heats for exhaust gas.

C. EGR Cooler Model

The EGR cooler is another lumped volume in the model. The pressure dynamics are modeled in the same manner as

used with the intake and exhaust manifolds.

$$\frac{dP_{egr}}{dt} = \frac{\gamma_{exh} R_{exh}}{V_{egr}} (W_{egr,in} T_{em} - W_{egr} T_{egr}) \tag{8}$$

The temperature of the EGR cooler outlet is assumed to be constant. The pressure drop across the EGR cooler is accounted for using the standard orifice flow equations, (6) and (7), where k in equation (6) is replaced with *egr,in*, corresponding to the flow into the EGR cooler. In equation (7), the upstream condition is the exhaust manifold and the downstream condition is the EGR cooler outlet conditions. The effective flow area and discharge coefficient are set to generate the correct pressure drop across the EGR cooler at a specified flow condition.

D. Charge Air Cooler Model

Again, just as the previous three lumped volumes were modeled, the charge air cooler model utilizes the same manifold filling dynamics.

$$\frac{dP_{cac}}{dt} = \frac{\gamma_{im} R_{im}}{V_{cac}} (W_{comp} T_{cac} - W_{cac} T_{cac}) \tag{9}$$

Similar to the EGR cooler, the CAC outlet temperature is assumed to be constant. The pressure drop across the CAC is also accounted for in the same way as that used in the EGR cooler model; the standard orifice flow equations, (6) and (7), are again implemented, where k in equation (6) can be replaced with *cac*. In equation (7), the upstream flow conditions are that of the compressor outlet and the downstream flow conditions are assumed to be that of the intake manifold.

E. Variable Geometry Turbocharger

The variable geometry turbocharger is modeled using turbine and compressor maps provided by the turbocharger manufacturer to determine the flow and efficiency of both the turbine and compressor. The turbine flow and the turbine efficiency are found with the turbine maps given the turbine inlet temperature, the pressure ratio across the turbine, the turbocharger shaft speed, and the nozzle position, shown in equation 10.

$$[W_{turb}, \eta_{turb}] = f(T_{em}, PR_{turb}, N_{turb}, X_{vgt}) \tag{10}$$

The turbine efficiency is represented by η_{turb}, PR_{turb} is the pressure ratio across the turbine, N_{turb} is the turbocharger shaft speed, and X_{vgt} is the turbine nozzle position. The turbine power is then calculated in equation 11.

$$P_t = W_{turb} c_{p,exh} \eta_{turb} T_{em} \left[1 - \frac{P_{amb}}{P_{em}} \right]^{\frac{\gamma_{exh}-1}{\gamma_{exh}}} \tag{11}$$

The input to the compressor maps to compute the compressor mass flow and efficiency include the turbocharger shaft speed, compressor inlet temperature, and the pressure ratio across the compressor, shown in equation 12.

$$[W_{comp}, \eta_{comp}] = f(N_{turb}, T_{amb}, PR_{comp}) \tag{12}$$

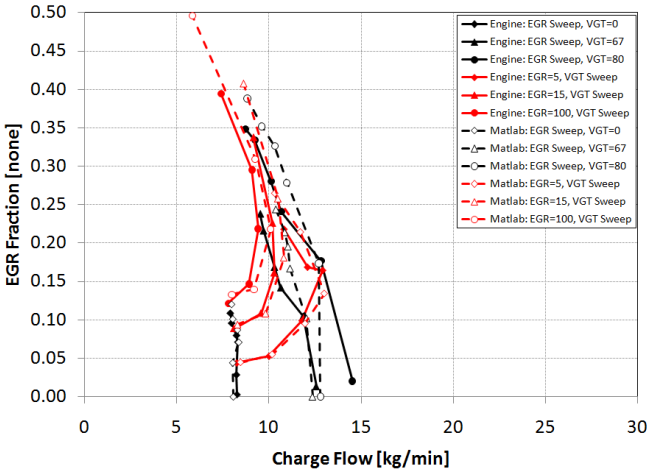

Fig. 2. Air Handling System Sweep at 1850 RPM and 300 ft-lb

The compressor power is then shown in equation 13.

$$P_{comp} = \frac{W_{comp} c_{p,amb} T_{amb}}{\eta_{comp}} \left[\left(\frac{P_{cac}}{P_{amb}} \right)^{\frac{\gamma_{amb}-1}{\gamma_{amb}}} - 1 \right] \tag{13}$$

The final model state equation is the turbocharger shaft speed. Using the turbine and compressor power in Newton's second law, the rate of change of the turbocharger shaft speed can be expressed as

$$\frac{dN_{turb}}{dt} = \frac{\eta_m P_{turb} - P_{comp}}{I_{turb} N_{turb}} \tag{14}$$

where I_{turb} is the moment of inertia of the turbochager. η_m is the mechanical efficiency of the turbocharger and is a function of the turbocharger shaft speed, $\eta_m = \eta_m(N_{turb})$.

IV. Steady State Results

The engine air handling system model is first compared to experimental engine data at steady state conditions. The model was validated against steady state engine data at an engine speed of 1850 RPM and torque of 300 ft-lb, shown in Figure 2, as well as at an engine speed of 2300 RPM and torque of 385 ft-lb, shown in Figure 3. In both cases, air handling system sweeps are performed that involve sweeping the EGR valve between 0% open and 100% open at three different positions of the VGT. The VGT sweeps are performed in the same way, with the VGT swept from 0% closed to 75% closed for three EGR valve positions.

The model accurately captures the trends from the air handling sweeps as demonstrated in Figures 2 and 3. Figure 2 shows that the model captures the trends as the EGR valve is opened, the EGR fraction increases while the charge flow decreases. The increase in EGR fraction is a result of more EGR flow as the EGR valve is opened. The reduction in charge flow as the EGR valve is opened is a result of more flow out of the exhaust manifold through the EGR valve, which results in the delivering of less energy to the turbine. Therefore, as the EGR valve is opened, the compressor is

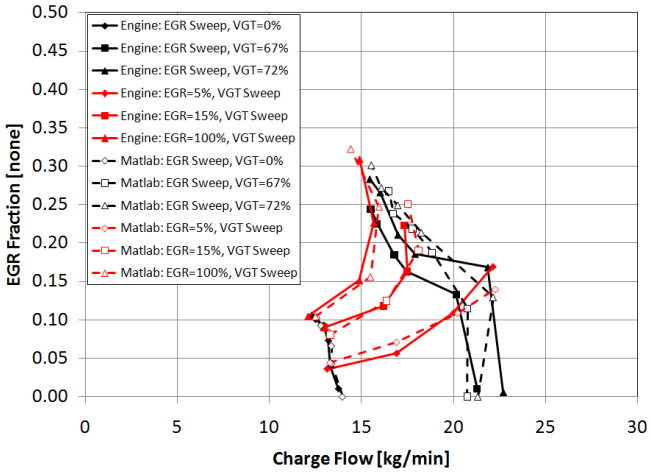

Fig. 3. Air Handling System Sweep at 2300 RPM and 385 ft-lb

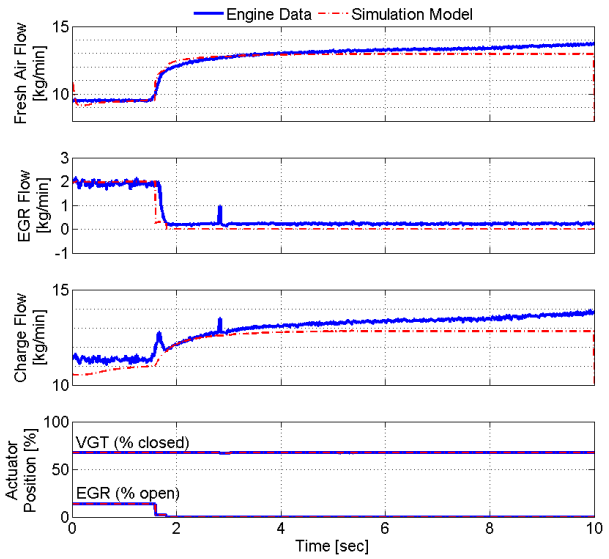

Fig. 4. System flows from a step change in the EGR valve position from 15% open to closed with the VGT at a constant 67% closed and at an engine speed of 1850 RPM and torque of 300 ft-lb

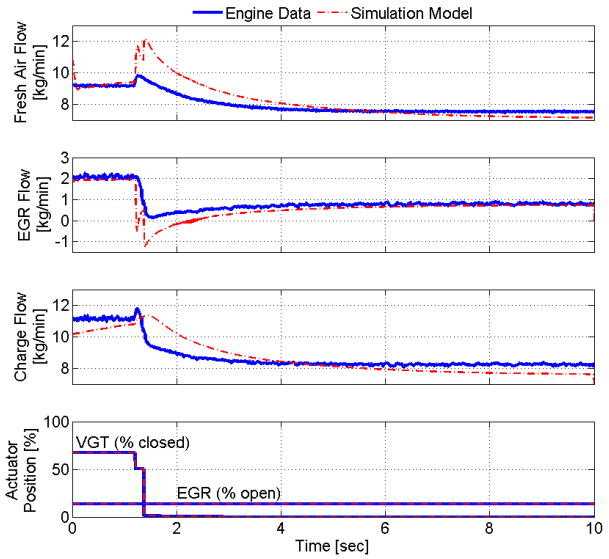

Fig. 5. System flows from a step change in the VGT position from 67% closed to open with the EGR valve at a constant 15% open and at an engine speed of 1850 RPM and torque of 300 ft-lb

receiving less power from the turbine to boost the incoming fresh-air charge. During the VGT sweeps, as the VGT is closed, the EGR fraction increases and the charge flow increases, in some cases, the charge flow will eventually begin to decrease. The increase in EGR fraction is due to more restriction to flow through the turbine, resulting in higher exhaust manifold pressures. For a fixed EGR position, increasing exhaust manifold pressures results in a greater pressure differential between the intake and exhaust manifolds, resulting in more EGR flow. The increase in charge flow is from both the increase in the EGR flow and the increase in the fresh air flow. The increase in fresh air flow is a result of an increase in turbocharger shaft speed due to the reduction in flow area through the turbine. The increased shaft speed results in more flow through the compressor, increasing the fresh air flow. The cases where the charge flow begins to decrease after closing the VGT beyond a certain point is a result of a decrease in the turbine efficiency, thus the power the turbine is able to provide decreases resulting in the compressor no longer being able to deliver as much fresh air flow.

Similar results are seen in Figure 3 for an engine speed of 2300 RPM and torque of 385 ft-lb. Again, the model accurately captures the trends as the EGR valve and VGT are swept through their respective ranges. In this case, the operating range of charge flows is larger, making the EGR fraction less sensitive to changes in the VGT position.

V. Transient Results

In order to test the model's transient predictive capabilities, it was compared to engine data at 1850 RPM and a torque of 300 ft-lb with step changes in either EGR position, VGT position, or both, shown in Figures 4, 5, and 6, respectively. As seen in all three sets of plots, the model and engine actuator (VGT and EGR) positions are exactly the same as these were inputs to the simulation model.

In Figure 4 the EGR valve was stepped from 15% open to a completely closed position while the VGT position was maintained at a 67% closed position. As is shown in the figure, the model-predicted fresh air flow and charge flow follow the engine data's transient response quite closely with very similar time constants. The initial error in the EGR flow immediately after the step change can be attributed to the error seen in the charge flow over the same time interval. The charge flow error is a result of the fresh air flow responding before the CO_2 measurements do. Therefore, for the short amount of time before the CO_2 measurements respond to the closed EGR valve, the EGR flow and fresh

air flow are both high. When the CO_2 measurements in the intake and exhaust manifolds begin to decrease due to the closed EGR valve, the charge flow falls back in line with the model-predicted values. The discrepancy in the charge flow at approximately 3 seconds was found to be noise in the intake CO_2 measurement. The steady state error in EGR flow can be attributed to the fact that when the EGR valve is completely closed, the model does not allow for any EGR flow through the valve, whereas the engine data shows that flow still occurs despite the valve being closed.

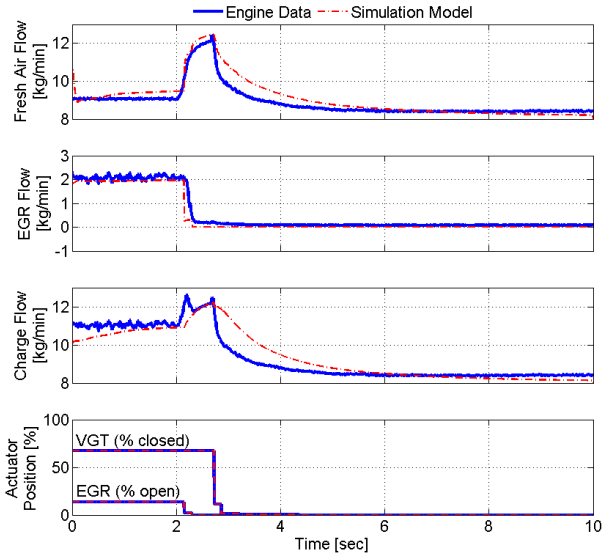

Fig. 6. System flows from a step change in the EGR position from 15% open to closed and the VGT position from 67% closed to open at an engine speed of 1850 RPM and torque of 300 ft-lb

More dynamic responses are observed with a step change in the VGT position, shown in Figure 5. The model predicts a larger transient response than what is seen in the engine data. As seen in the fresh air flow plot in Figure 5, the model correctly predicts an initial increase in fresh air flow before ultimately decreasing to steady state conditions. Similarly, the model captures the initial undershoot of the change in EGR flow before ultimately reaching a steady state value lower than before the step change. The charge flow response similarly follows the fresh air flow response, with an initial increase, before ultimately converging on a steady state value lower than that before the step change. Not only does the model capture the dynamic behavior of the step change, but it also converges on steady state values very close to the actual engine data.

When both actuators are used to exercise the model during a single simulation, the model still performs very well. Figure 6 shows the system flows for both the simulation model and engine data. As shown in the figure, when the EGR valve is closed, the model responds very accurately to the changes in fresh air flow and EGR flow. The charge flow simulation results are slower than the actual engine data, but the EGR flow performs a step change in the simulation,

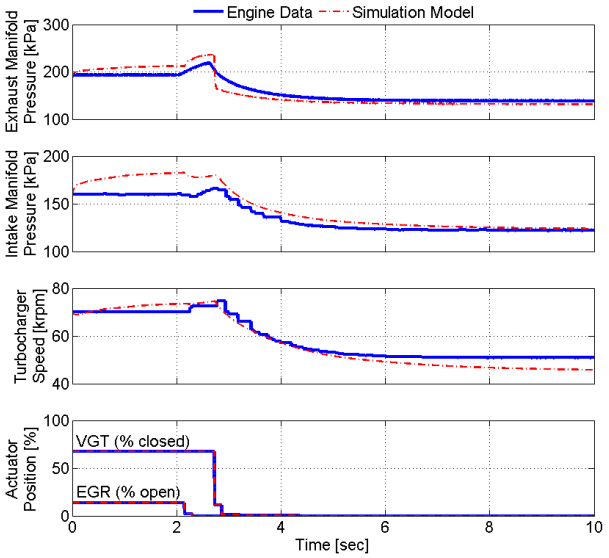

Fig. 7. System pressures from a step change in the EGR position from 15% open to closed and the VGT position from 67% closed to open at an engine speed of 1850 RPM and torque of 300 ft-lb

whereas the engine data is slower. This slight discrepancy in the EGR flow accounts for the initial error on the charge flow. When the VGT actuator is stepped from 67% closed to 100% open, the model does not respond as quickly as the engine data, but the model does converge to steady state values very close to the actual engine data. The predictive capability of the model also extends to the manifold pressure dynamics, shown in Figure 7. The model accurately predicts the intake and exhaust manifold pressures as well as the turbocharger shaft speed. The transient error in the exhaust manifold pressure is a result of the response time of the pressure transducer.

VI. Conclusions and Future Work

This paper presents a physically motivated reduced order model of the air handling system of a modern diesel engine, to be used for control design. Model results have been compared with corresponding engine test data and the model satisfactorily demonstrates the ability to closely emulate the physical response of the engine, during both steady state and transient operation. This control oriented model is intended for the development of closed-loop control and estimation strategy that will ultimately leverage the capabilities of the variable valve actuation system to explore novel combustion strategies.

Future work identified includes incorporating a temperature predictive combustion model as well as a physics based volumetric efficiency model that will also be a function of intake valve closure time. The engine test-bed measurements will also be examined for areas of improvement, specifically high bandwidth pressure transducers for the intake and exhaust manifold.

VII. Acknowledgement

This material is based upon work supported by the Department of Energy under Award Number DE-EE0003403.

VIII. Disclaimer

References

[1] X. Yang and G. G. Zhu, "A mixed mean-value and crank-based model of a dual stage turbocharged si engine for hardware-in-the-loop simulation," *Proceedings of the 2010 American Control Conference*, 2010.

[2] F. Yan and J. Wang, "In-cylinder oxygen mass fraction cycle-by-cycle estimation via a lyapunov-based observer design," *Proceedings of the 2010 American Control Conference*, 2010.

[3] J. Wang, "Hybrid robust air-path control for diesel engines operating conventional and low temperature combustion modes," *IEEE Transactions of Control Systems Technology*, 2008.

[4] A. Plianos and R. Stobard, "Modeling and control of diesel engines equipped with a two-stage turbo-system," *SAE 2008-01-1018*, 2008.

[5] D. Stanton, "Analysis led design for engine system development to meet US2010 emissions standards," *Presentation at the Wisconsin Engine Research Center (ERC)*, 2005.

[6] L. Pickett and D. Siebers, "Soot formation in diesel fuel jets near the lift-off length," *International J. of Engine Research*, vol. 7, 2006.

[7] L. Pickett, S. Kook, H. Persson, and O. Andersson, "Diesel fuel jet lift-off stabilization in the presence of laser-induced plasma ignition," *Proc. of the Comb. Inst.*, vol. 32, pp. 2793–2800, 2009.

[8] L. Guzzella and A. Amstutz, "Control of diesel engines," *IEEE Control Systems Magazine*, vol. 18, no. 5, pp. 53–71, 1998.

[9] W. Eckerle and D. Stanton, "Analysis-led design process for Cummins engine development," *THIESEL*, 2006.

[10] M. Kao and J. Moskwa, "Turbocharged diesel engine modeling for nonlinear engine control and state estimation," *Dynamic Systems, Measurement, and Control*, vol. 117, 1995.

[11] Y. He, "Development and validation of a 1d model of a turbocharged v6 diesel engine operating under steady-state and transient conditions," *SAE 2005-01-3857*, 2005.

[12] Y. He, C.-C. Lin, and A. Gangopadhyay, "Integrated simulation of the engine and control system of a turbocharged diesel engine," *SAE 2006-01-0439*, 2006.

[13] A. Kulkarni, G. M. Shaver, S. Popuri, T. R. Frazier, and D. W. Stanton, "Computationally efficient whole-engine model of a cummins 2007 turbocharged diesel engine," *J. Eng. Gas Turbines Power,Volume 132, Issue 2, 022803*, 2009.

[14] T. Morel, R. Keribar, J. Silvestri, and S. Wahiduzzaman, "Integrated engine/vehicle simulation and control," *SAE 1999-01-0907*, 1999.

[15] C. Ciesla, R. Keribar, and T. Morel, "Engine/powertrain/vehicle modeling tool applicable to all stages of the design process," *SAE 2000-01-0934*, 2000.

[16] I. Kolmanovsky and M. v. N. P. Moraal, "Issues in modelling and control of intake flow in variable geometry turbocharged engines," *Proceedings of the 18th IFIP conference on system modeling and optimization*, 1997.

[17] M. Jankovic, M. Jankovic, and I. Kolmanovsky, "Constructive lyapunov control design for turbocharged diesel engines," *IEEE Transactions of Control SystemsTechnology*, 2000.

[18] M. Ammann, N. P. Fekete, L. Guzzella, and A. H. Glattfelder, "Model-based control of the vgt and egr in a turbocharged common-rail diesel engine: Theory and passenger car implementation," *SAE 2003-01-0357*, 2003.

[19] H. Das and S. Dhinagar, "Airpath modelling and control for a turbocharged diesel engine," *SAE 2008-01-0999*, 2008.

[20] A. G. Stefanopoulou, I. Kolmanovsky, and J. S. Freudenberg, "Control of variable geometry turbocharged diesel engines for reduced emissions," *IEEE Transactions of Control System Technology, Volume 8, NO. 4, July 2000*, 2000.

[21] M. Canova, S. Midlam-Mohler, Y. Guezennec, and G. Rizzoni, "Mean value modeling and analysis of hcci diesel engines with external mixture formation," *Dynamic Systems, Measurement, and Control*, vol. 131, 2009.

[22] J. Heywood, *Internal Combustion Engine Fundamentals*. New York, NY USA: McGraw-Hill, 1998.